

Rethinking pose estimation in crowds: overcoming the detection information-bottleneck and ambiguity

Mu Zhou*

Lucas Stoffl*

Mackenzie Mathis

Alexander Mathis

Ecole Polytechnique Fédérale de Lausanne (EPFL)
alexander.mathis@epfl.ch

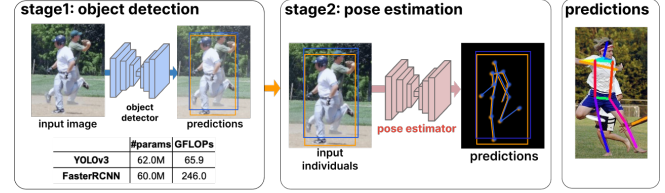
Frequent interactions between individuals are a fundamental challenge for pose estimation algorithms. Current pipelines either use an object detector together with a pose estimator (top-down approach), or localize all body parts first and then link them to predict the pose of individuals (bottom-up). Yet, when individuals closely interact, top-down methods are ill-defined due to overlapping individuals, and bottom-up methods often falsely infer connections to distant body parts. Thus, we propose a novel pipeline called bottom-up conditioned top-down pose estimation (BUCTD) that combines the strengths of bottom-up and top-down methods. Specifically, we propose to use a bottom-up model as the detector, which in addition to an estimated bounding box provides a pose proposal that is fed as condition to an attention-based top-down model. We demonstrate the performance and efficiency of our approach on animal and human pose estimation benchmarks. On CrowdPose and OCHuman, we outperform previous state-of-the-art models by a significant margin. We achieve 78.5 AP on CrowdPose and 47.2 AP on OCHuman, an improvement of 8.6% and 4.9% over the prior art, respectively. Furthermore, we show that our method has excellent performance on non-crowded datasets such as COCO, and strongly improves the performance on multi-animal benchmarks involving mice, fish and monkeys. The code is available at <https://github.com/amathislab/CondTopDown>.

Introduction

Imagine somebody hands you an image of a person and asks you “to annotate the pose”. For your exquisite primate visual system this is a trivial task that you can readily achieve. Now imagine somebody hands you another image that contains two people, arm-in-arm. You are likely frustrated and will ask whose pose you should annotate. In response to whose pose you should annotate, your instructor will likely point at the person they have in mind. Based on the pointing, it is again easy to annotate the right individual’s pose. Our work proposes a hybrid deep learning framework for pose estimation that is inspired by this interaction.

This simple example highlights the ambiguity problem of top-down approaches in crowds. They first localize individuals with a dedicated object detector (1–4) and then perform single-instance pose estimation (5–11). In contrast,

Top-down approach



Our hybrid approach (BUCTD)

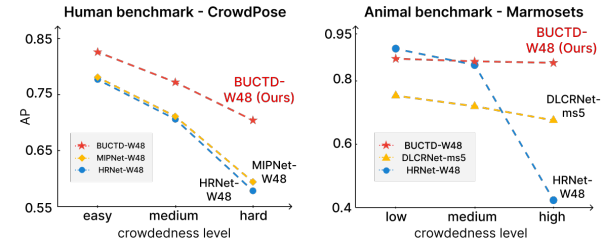
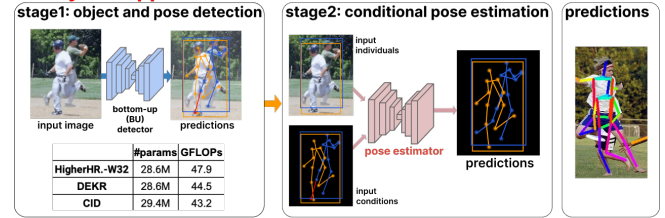


Fig. 1. Overview of our bottom-up conditioned top-down pose estimation (BUCTD) approach and benchmarking results. BUCTD uses a bottom-up pose model as instance detector, which is computationally cheaper than existing, widely-used object detectors. The pose proposals from the pose detector are used to calculate bounding boxes and to condition our novel, conditional top-down stage on. Note that, as in a standard top-down paradigm, only one image crop plus its corresponding conditional pose is presented to the BUCTD. We can substantially boost performance on both human and animal benchmarks, with especially large gains in crowded scenes.

bottom-up approaches first localize body parts in the image and then assemble them into poses of each of the individuals simultaneously (12–18). Yet, when individuals closely interact, top-down methods are ill-defined as it is unclear which pose should be predicted within a bounding box that contains multiple individuals. Therefore, occluded individuals will often be ignored by top-down methods (Figure 1). In contrast, as bottom-up approaches reason over the complete scene they may not have this problem. Bottom-up approaches can localize all individuals, but often struggle with accurate predictions for occluded poses.

To overcome those limitations we propose a hybrid

*These authors contributed equally to this work

framework called **Bottom-Up Conditioned Top-Down** pose estimation (BUCTD). Our solution is inspired by the interaction that we described. Instead of using object detectors, we propose to use bottom-up pose estimation models as detectors. The output poses are used to estimate bounding boxes of the individuals, and also serve as a “pointing” mechanism, that indicates whose pose should be predicted. To also process the “pointing” input, we generalize top-down models to conditional-top down (CTD) models, which present the second stage of our BUCTD framework. CTD take a cropped image together with a pose as input. CTD models are then trained to predict the correct pose based on the (potentially) noisy pose provided by the bottom-up methods (Figure 1).

Thus, BUCTD overcomes the information bottleneck and ambiguity introduced by standard detectors, while typically having similar or lower inference cost (Figure 1). We evaluate BUCTD on COCO (19), two crowded human benchmarks, CrowdPose (8) and OCHuman (20), and three multi-animal benchmarks, namely SchoolingFish, Tri-Mouse and Marmosets (17). We achieve state-of-the-art (SOTA) performance on the crowded human benchmarks and animal benchmarks, and strongly outperform both top-down and bottom-up models in occluded and crowded scenes.

Related Work

Multi-instance pose estimation and benchmarks. Top-down approaches detect the body parts of each individual by a single-instance pose estimation model (5–7) within the detected bounding box generated by the object detector (1–4, 21). Recently, transformer-based top-down methods such as TransPose (9), TokenPose (10), TFPose (22) and ViTPose (11) have increased the performance. Exemplar bottom-up approaches include OpenPose (13), Associative Embedding (14), ArtTrack (12), HigherHRNet (15), DEKR (16), DLCRNet (17) and PETR (18).

Classic benchmarks for human pose estimation, such as COCO (19) and MPII (23), contain few occlusions (24), even though this is typical in many real-world scenarios. In recent years new benchmarks with more crowded scenes emerged, most notably CrowdPose (8) and OCHuman (20). Interestingly, multi-animal pose estimation benchmarks share some of the challenges of human benchmarks, but also raise other problems (25), such as highly similar appearance within a given species, such as mice. Therefore, to tackle these challenges we also focused on multi-animal benchmarks comprising mice, monkeys, and groups of fish with heavy overlap (17). Our method, BUCTD, achieves SOTA on all these benchmarks.

Combination of Top-Down and Bottom-Up Models. Hu and Ramanan (26) proposed a bidirectional architecture for hierarchical Rectified Gaussian models incorporating top-down feedback with bottom-up architecture, while Tang et al. (27) introduced an hierarchical, compositional model and a bone-based part representation for human pose estimation, where the inference process consists of both bottom-up and top-down stages across multiple semantic levels. Cai et

al. (28) developed a novel graph-based method for 3D pose estimation by concatenating the bottom-up features and top-down features together. Li et al. (29) proposed to use bottom-up methods to estimate the joints and leverage the bounding boxes from a top-down detector to group the joints, while Cheng et al. (30) shows another, similar way to combine top-down and bottom-up approaches. In these methods, estimated joints from top-down approaches are fed to a bottom-up network, which make use of visual features to refine the poses. In comparison to previous works, and instead of using an object detector, our BUCTD leverages bottom-up models as detectors which have less computational costs and provide a ‘pointer’ to guide the model to pay attention to the correct target individual, that is especially effective in crowded scenes.

Crowded scene pose estimation. Many recent works (8, 20, 24, 31) have focused on occluded scenes in pose estimation. Khirodkar et al. (24) propose a hybrid top-down approach called MIPNet, which allows the model to predict multiple people within a given bounding box. MIPNet reached SOTA performance by providing an integer input to indicate which human with respect to the distance from the center should be predicted. In contrast, we hypothesize that providing a pose cue about which individual should be predicted is advantageous. The CID model (32) proposes an end-to-end architecture including a CNN backbone and a feature decoupling stage to distinguish between individuals. However, the decoupling is only based on the center prediction of individuals. CenterGroup (33) uses attention to link person centers to body parts, while PETR (18) deploys separate, transformer-based decoders for individuals and keypoints respectively. Ding et al. (34) recently proposed another attention-based model that appears to have strong performance on CrowdPose and OCHuman. However, the authors evaluate their model differently than the field, i.e., only based on ground-truth bounding boxes, and hence we do not compare it to other approaches. For the first stage of BUCTD, we are building on the latest bottom-up methods, such as CID (32), and PETR (18). For the second stage, we generalized top-down models to conditional top-down models (CTD). Instead of an index as in MIPNET (24), we provide a “pointer” in the form of a pose predicted from a bottom-up model. Thus, our CTD model gets two inputs: a bounding box and a pose similar in spirit to PoseFix (35) or PoseRefiner (36). Akin to PoseFix and PoseRefiner we also test a convolutional PreNet that provides the pose at the early stage of the top-down model. Moreover, we also develop transformer and attention based models for providing the conditional input. We find that they achieve better performance and are more efficient. How is the conditional input provided? We either sample it from the known error distributions (37), or sample it based on the predictions of the BU models. As we will show, both approaches provide strong results.

Methods

BUCTD framework. Our BUCTD model is a two-stage model trained to predict the pose from the cropped input im-

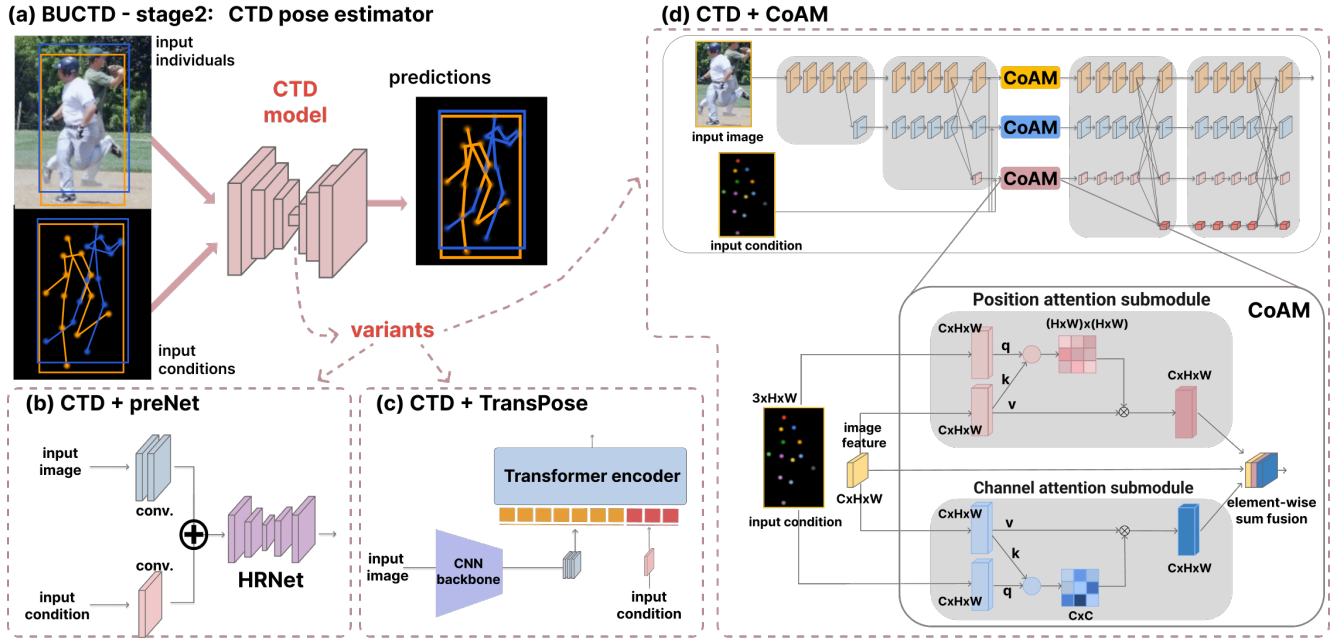


Fig. 2. Overview of the second stage of our BUCTD approach: conditional top-down (CTD) pose estimators. (a) CTD receives a conditional pose and a cropped image, whose crop was estimated from the conditioned keypoints. (b) CTD with preNet. (c) CTD with TransPose. (d) CTD with Conditional Attention Module (CoAM). (**Top:** Our CTD model simply employs the same multi-resolution stages as the standard HRNet; we insert our CoAM module after stage 2 (one CoAM for every resolution branch). **Bottom:** CoAM. The output of stage 2 for one branch (image feature) is treated as keys and values for the two attention submodules, while we feed the color-coded condition heatmap as queries into the attention mechanisms. The output of the module is a combination of the spatial attention feature, the channel attention feature and the original image feature.

age and the bottom-up input (Figure 2). Importantly, our training scheme differs from classic top-down approaches, since we train on cropped images generated from the bottom-up pose predictions, in contrast to using the ground-truth bounding boxes. This induces additional augmentation in the training. The intuition is that BUCTD can use the image as well as the pose input to know which individual to predict. This overcomes the inherent ambiguity for top-down approaches in crowded scenes.

Stage1: Bottom-Up detector (BU). Firstly, to detect individuals, we use a bottom-up pose estimation model on the target training dataset and get the predictions. Classic top-down methods use a generic object detector to get the bounding boxes for individuals; however, bounding boxes create an information bottleneck between the detector and the pose estimation model. Furthermore, in real-world applications, training an object detector has higher computational cost compared to training bottom-up pose models (Figure 2). Therefore, we propose to use a bottom-up model as the detector, which will provide both a predicted pose as guidance, and the corresponding bounding box. Of course, also recent single-stage models (18, 32) can (and will) be used.

Stage2: Conditional Top-Down (CTD). Secondly, we train CTD models with the conditional pose input and the corresponding bounding box. During training, we experiment with two different sampling strategies for the conditions. 1) **Empirical sampling:** We sample the conditions from the predictions of BU models, where we match the ground truth pose with those predictions by using Object Keypoint Similarity (OKS) on human benchmark and bounding box IoU on ani-

mal benchmark. 2) **Generative sampling:** Instead of taking actual predictions, one can also synthetically sample input poses based on estimated error distributions of pose estimation algorithms (37). This approach is similar as shown in PoseFix (35).

CTD model architectures. The second stage of our BUCTD approach consists of conditional top-down (CTD) pose estimation models, that provide a generic solution to tackle multi-instance pose estimation in crowded scenes. In this section, we describe the flexibility of the BUCTD approach by adopting different CTD architectures (Figure 2a-d). In all cases, we convert the conditional input from the predicted keypoints into a 3-channel heatmap by using a Gaussian distribution with a standard deviation σ . To keep the semantic information, we provide each keypoint with a certain RGB value. We empirically found that the colored heatmap worked best compared to other choices (see Suppl. Mat. A.3).

CTD with a Conditional Attention Module. To learn a better representation and leverage the information from the conditional input, we propose an architecture comprised of HRNet (7) and a Conditional Attention Module (CoAM; Figure 2d), where we feed the input image and the corresponding pose condition into HRNet and the CoAM in parallel. The CoAM can be inserted after any HRNet-stage and its output is fused with the features of the corresponding stage. Unless otherwise indicated the CoAM input was placed after HRNet-stage two. Therefore, the conditional input (1) provides a clue to which individual in the crop the CTD model should focus on, (2) improves the input pose obtained from the bottom-up model.

CoAM is inspired by Fu et al. (38) and contains spatial and channel attention sub-modules. It is designed to learn associations between features and “conditions” with an attention-like mechanism. Finally, it aggregates and fuses the features from both sub-modules by performing an element-wise sum. The resulting feature map is added back to the module’s input feature map, hence combining the features extracted from the HRNet with the long-range contextual information. The CoAM module treats the conditions as queries and the feature maps as keys and values for calculating the attention scores (Figure 2d). We note that the CoAM module could also be combined with other CNN models.

Position Attention Module. Given a local feature f , we first feed it into a convolution layer to obtain $F \in \mathbb{R}^{C \times H \times W}$ and embed it linearly to generate two new features maps K and V (keys and values) with $K, V \in \mathbb{R}^{C \times H \times W}$. The condition heatmap $c \in \mathbb{R}^{3 \times H \times W}$ at the corresponding stage is also processed by a convolution layer to create $C \in \mathbb{R}^{3 \times H \times W}$ and embedded linearly into Q (queries) with $Q \in \mathbb{R}^{C \times H \times W}$. We reshape queries, keys and values to $\mathbb{R}^{C \times N}$, where $N = H \times W$ is the number of pixels. A softmax layer is applied after a matrix multiplication between the transpose of Q and K , to generate the spatial attention map $S \in \mathbb{R}^{N \times N}$:

$$s_{ji} = \frac{\exp(Q_i \cdot K_j)}{\sum_{i=1}^N \exp(Q_i \cdot K_j)} \quad (1)$$

where s_{ji} measures the impact of condition position i on the feature position j . Then, we perform a matrix multiplication between V and the transpose of S and reshape the result to $\mathbb{R}^{C \times H \times W}$ to obtain the final output P of the position attention submodule:

$$P_j = \sum_{i=1}^N (s_{ji} V_i) \quad (2)$$

The resulting feature from the position attention submodule has a global contextual view and aggregates the conditional context according to the spatial attention map.

Channel Attention Module. Each channel map of high level features can be regarded as a keypoint-specific response while the condition itself is a keypoint-specific map. Hence, it is beneficial to learn the associations between these different semantic representations.

Different from the position attention submodule, the channel attention submodule directly calculates the channel attention map $X \in \mathbb{R}^{C \times C}$ from the original features F (treated as key and value) and the condition C (processed by convolution layer to be in $\mathbb{R}^{C \times H \times W}$ and treated as query). Specifically, we reshape both F and C to $\mathbb{R}^{C \times N}$, and then perform a matrix multiplication between F and the transpose of C , followed by a softmax layer to retain the channel attention map $X \in \mathbb{R}^{C \times C}$:

$$x_{ji} = \frac{\exp(C_i \cdot F_j)}{\sum_{i=1}^C \exp(C_i \cdot F_j)} \quad (3)$$

where x_{ji} measure the impact of the condition channel i on the feature channel j . Afterwards, we perform a matrix mul-

tiplication between the transpose of X and F and reshape the result to $\mathbb{R}^{C \times H \times W}$ to obtain the final output E of the channel attention submodule:

$$E_j = \sum_{i=1}^C (x_{ji} F_i) \quad (4)$$

The final feature of the channel attention submodule models the long-range semantic dependencies between conditional keypoints and feature maps.

To obtain the final output M of CoAM, we perform an element-wise sum operation between the original feature map F and the outputs of the respective submodules P and E :

$$M_j = F_j + (P_j + E_j) \quad (5)$$

CTD with preNet. Given an input pair comprising an input image and input condition, we feed the pair in parallel to the preNet which contains two different convolutional layers, to extract features from both inputs (i.e., two 7x7 conv. layers for input image and one 7x7 conv. layer for the conditional input). Then, we fuse the image feature and the condition feature together and feed it into either HRNet-W32 or W48 (7). Thus, CTD-preNet-W32 or W48 is a simple architecture leveraging the CTD approach (Figure 2b).

CTD with TransPose. We modified the TransPose (9) architecture to leverage its powerful transformer architecture. TransPose consists of a CNN backbone whose output features are transformed to $d \times H \times W$ by a 1×1 convolution. These image feature maps are then flattened into a sequence $X \in \mathbb{R}^{N \times d}$, with $N = H \times W$, which is then fed to a standard transformer encoder. For CTD+TransPose, we provide condition as “side-information” by concatenating condition-specific tokens to this transformer input sequence (Figure 2c). Specifically, we transform the conditional heatmap first by a 1×1 convolution to expand the number of channels to c and, after flattening, obtain a condition sequence $Y \in \mathbb{R}^{N \times c}$. Here, we somewhat arbitrarily chose $c = 16$. The final input sequence to the transformer encoder is the concatenation of X and Y , i.e., $X \oplus Y$. The attention layers enable capturing long-range relationships between the conditional input and the predicted keypoints.

Implementation details

BUCTD with CoAM. We trained HRNet-W32 (7) and HRNet-W48 (7) with CoAM (BUCTD-CoAM-W32 and CoAM-W48) on all benchmarks. Results of CoAM-W32 and CoAM-W48 are reported to verify the strong performance of BUCTD in several benchmarks.

BUCTD with preNet. We equipped HRNet-W48 (7) with a preNet to train BUCTD-preNet-W48 and report the efficiency on the animal benchmarks. We also used BUCTD-preNet-W32 for the human benchmarks.

BUCTD with TransPose. We trained our BUCTD-TP-H-A6 model (based on the TransPose-H-A6 architecture (9)) on CrowdPose to show that the conditional top-down approach

can be successfully integrated into transformers. Additional details for all models can be found in the Suppl. Mat. A.

Training Details. To obtain the conditional inputs for training our models with empirical sampling, we trained bottom-up pose estimation models, DLCRNet (17) for animal pose, and HigherHRNet (15) for CrowdPose and OCHuman, and saved (pose) predictions from different model checkpoints (animals: up to 8-12 checkpoints, human: 15 checkpoints).

During training and inference, we enlarged the bounding box by adding a fixed margin (25 pixels) in height and width to the predicted bounding box, for animal datasets. In addition, we also augmented the bounding boxes during training by random scaling the enlarged box. To keep the aspect ratio and avoid distortion of the animal’s body, we resized and padded the predicted bounding box to 256×256 . For the human data, we used a margin of 5 pixels and extend each detection box to a fixed aspect ratio (256×192 or 384×288). We followed the same training scheme (batch size, learning rate, weight initialization, augmentation scheme, loss function) as in (7, 24). As for the experiments using generative sampling strategy, we use the same error distribution as in PoseFix (35, 37) on human benchmarks and adapted it for animal benchmarks.

Experiments

To evaluate BUCTD, we performed comprehensive experiments on several benchmarks. We tested our approach on the most important benchmarks for crowded scenes (CrowdPose (8) and Occluded Human (OCHuman) (20)), a common but less crowded benchmark, COCO (19), as well as on three multi-animal pose estimation benchmarks (17). We also carried out several ablations to test the design choices.

CrowdPose Benchmark

Dataset. The CrowdPose dataset (8) contains 12K labeled images in the *trainval* set with 43.4K labeled persons (each with 14 keypoints), and 8K images in the *test* set with 29K labeled persons. Following other studies (16, 18, 32), we used *trainval* for training, and *test* for evaluation. We report standard metrics AP, AP_{easy} , AP_{med} and AP_{hard} as defined in (8). We compared our method, that derives bounding boxes from a bottom-up model (see Methods), with baselines that used bounding boxes obtained by a Faster R-CNN (2) detector.

Results. We compared BUCTD to bottom-up, single-stage, and top-down methods. Overall, BUCTD achieved SOTA performance on this benchmark (Table 1, Figure 3). Strikingly, we improved upon MIPNet-W48 (24) by up to 8.5 AP. To achieve these results, BUCTD-W48 was trained with bottom-up predictions from HigherHRNet-W32 (15) (which alone performs relatively poorly) and generative sampling. This begs the question, can BUCTD-W48 generalize to conditional inputs from other models? To test this, we evaluated the test-performance (without re-training) of BUCTD-W48 when it was provided with inputs from recently de-

scribed SOTA bottom-up or single-stage models (CID-W32 and PETR, respectively). We found strong performance gains for both models (Table 1). Overall, BUCTD achieves substantial performance gains with the same backbone (CID-W48 vs. BUCTD-W48++ showed a 6 AP gain in performance).

Next we evaluated other second-stage, CTD, architectures on CrowdPose. We found that all methods could increase the performance and generalized to other bottom-up pose estimation model inputs (Table 2). Using the CoAM module provided the best results, and outperformed the CTD-preNet models, which can be seen as an updated version of PoseFix (35). This suggests that our hybrid approach indeed combines the strengths of both bottom-up and top-down methods.

BUCTD achieved stronger performance than other hybrid approaches. Does that gain come at the cost of higher computational cost? Training and performing inference is comparable for object detectors and BU models, as BU models often have similar or fewer parameters and GFLOPs (Table S5). Moreover to gain additional insights, we computed the precision and recall for the BUCTD approach for different BU models on CrowdPose (Figure S2). We compare our model to the previous SOTA on CrowdPose: MIPNet. Importantly, BUCTD has higher recall and precision than MIPNet for all models. Interestingly, some BU models provide more detections than detectors. To fairly compare, we also provided exactly the same number of detections from both the bottom-up models and an object detector; despite this artificial constraint the performance of BUCTD was still significantly higher than the one of MIPNet (24), indicating that the performance gains are not simply coming from a higher number of provided detections (Figure S3).

Method	Input size	AP	AP_{easy}	AP_{med}	AP_{hard}
Bottom-Up methods					
HRNet-W48 (7)	640	67.3	74.6	68.1	58.7
HigherHRNet-W48 (15)	640	67.6	75.8	68.1	58.9
CenterGroup (33)	640	69.4	76.6	70.0	61.5
BAPose (39)	512	72.2	79.9	73.4	61.3
Single-stage methods					
DEKR (16)	640	68.0	76.6	68.8	58.4
PETR (18)	800	72.0	78.0	72.5	65.4
CID-W32 (32)	512	71.3	77.4	72.1	63.9
CID-W48 (32)	640	72.3	78.7	73.0	64.8
Top-Down methods					
AlphaPose (5)	-	61.0	71.2	61.4	51.1
JC-SPPE (8)	320×256	66.0	75.5	66.3	57.4
HRNet-W48 (7)	384×288	69.3	77.7	70.6	57.8
Hybrid approaches					
MIPNet-W48 (24)	384×288	70.0	78.1	71.1	59.4
BUCTD-W48 (Ours)	384×288	72.9	79.2	73.4	66.1
BUCTD-W48+ (Ours)	384×288	75.3	81.1	75.9	68.4
BUCTD-W48++ (Ours)	384×288	76.7	82.6	77.2	70.4
BUCTD-W48+++ (Ours)	384×288	78.5	83.9	79.0	72.3

Table 1. BUCTD improved performance on CrowdPose *test* set. First three BUCTD models are trained with HigherHRNet-W32 conditions. All BUCTD models are based on a HRNet-W48, and include CoAM. + denotes cond. input from CID-W32, ++ denotes cond. input from PETR, and * denotes generative sampling.

Ablation Results. To validate our design choices we performed ablation studies on the CTD-CoAM-W32 model. We

(a) Qualitative results



(b) Comparison results

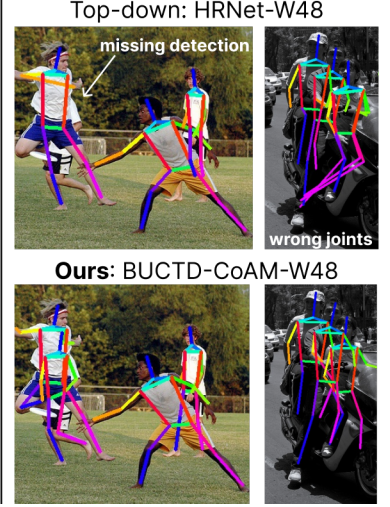


Fig. 3. Results using BUCTD on crowded images. (a) Qualitative results on CrowdPose (top row) and OCHuman (bottom row) with our BUCTD method. (b) Top: predictions from top-down approach, bottom: predictions from our BUCTD model. The images are from the Crowdpose test set.

experimented with the position of CoAM and found that conditional inputs are best provided at earlier stages in the network (Table 3). We further wanted to validate the impact of different conditional inputs during training. In comparison to the 15 checkpoints we obtained from training the bottom-up model (HigherHRNet-W32), we trained CTD models with conditions from different numbers and types of conditions (Table 4). Generally speaking, CTD models can better learn to predict poses when they are trained with diverse conditional poses for empirical sampling; generative sampling can further improve the performance.

Method	AP	AP _{easy}	AP _{med}	AP _{hard}
HigherHRNet-W32 (15)	65.7	73.2	66.1	57.9
CTD-preNet-W32†	69.5 (+3.8)	76.2	69.9	62.5 (+4.6)
CTD-TP-H-A6†	70.7 (+5.0)	77.9	71.1	63.0 (+5.1)
CTD-CoAM-W32†	71.4 (+5.7)	78.0	71.8	64.5 (+6.6)
CTD-CoAM-W48★	72.9 (+7.2)	79.2	73.4	66.1 (+8.2)
DEKR (16)	68.0	76.6	68.8	58.4
CTD-preNet-W32†	69.7 (+1.7)	77.7	70.6	60.5 (+2.1)
CTD-TP-H-A6†	71.0 (+3.0)	79.1	71.9	61.7 (+3.3)
CTD-CoAM-W32†	71.1 (+3.1)	78.8	71.9	61.8 (+3.4)
CTD-CoAM-W48★	72.0 (+4.0)	79.5	72.8	63.0 (+4.6)
CID-W32 (32)	71.3	77.4	72.1	63.9
CTD-preNet-W32†	72.8 (+1.5)	79.0	73.4	65.7 (+1.8)
CTD-TP-H-A6†	73.7 (+2.4)	80.1	74.5	66.2 (+2.3)
CTD-CoAM-W32†	74.2 (+2.9)	80.2	74.9	67.1 (+3.2)
CTD-CoAM-W48★	75.3 (+4.0)	81.1	75.9	68.4 (+4.5)
PETR (18)	72.0	78.0	72.5	65.4
CTD-preNet-W32†	74.6 (+2.6)	80.9	75.1	67.7 (+2.3)
CTD-TP-H-A6†	75.6 (+3.6)	82.2	76.1	68.6 (+3.2)
CTD-CoAM-W32†	75.9 (+3.9)	81.9	76.3	69.1 (+3.7)
CTD-CoAM-W48★	76.7 (+4.7)	82.6	77.2	70.4 (+5.0)

Table 2. CTD boosts CrowdPose results for different variants using conditional inputs from different bottom-up and single-stage models (on *test* set). † and ★ denotes input resolution of 256x192 and 384x288 respectively. All CTD models are trained with HigherHRNet-W32 conditional input.

Method	stage	AP	AP _{easy}	AP _{med}	AP _{hard}
BUCTD-CoAM-W32	1	71.2	77.8	71.6	64.2
BUCTD-CoAM-W32	2	71.2	77.7	71.6	64.3
BUCTD-CoAM-W32	3	70.5	77.4	70.9	63.3
BUCTD-CoAM-W32	4	68.3	76.8	69.2	58.7

Table 3. Ablating the position of CoAM on CrowdPose *test*. Feeding the conditions through CoAM in earlier stages of the HRNet architecture increased performance.

OCHuman Benchmark

Dataset. The OCHuman dataset (20) is the most challenging dataset for crowded multi-person pose estimation with an average of 0.67 MaxIoU (Intersection over Union between bounding boxes) for each person, which contains 4,731 images with 8,110 persons in total. For a fair comparison, we report the results in the same way as illustrated in (20, 32), namely we train our models on the COCO *train* set and evaluate on OCHuman *test* set.

Results. Previous SOTA results on OCHuman were reported by the single-stage model CID (32). We reach new SOTA performance, with gains ranging from 2.2 to 7.8 AP, depending on the baseline (top-down or bottom-up). BUCTD outperforms baseline models, even with a lower input resolution, and a smaller HRNet backbone (BUCTD-W32). Particularly notable are the gains over bottom-up methods, which historically do well in crowded scenes, and over the recently introduced strong single-stage method CID (32). Qualitative results can be seen in Figure 3a.

COCO Benchmark

Dataset. The COCO (19) dataset contains 57K images with 150K persons in the *train* set, 5K images with 6.3K persons in the *val* set and 20K images in the test-dev set. We used *train* for training and *val* for validation. We compared our method with several bottom-up models and top-down meth-

GT	#checkpts HrHRNet	#checkpts DEKR	#checkpts CID	#checkpts PETR	AP	AP _{easy}	AP _{med}	AP _{hard}	AP	AP _{easy}	AP _{med}	AP _{hard}
					Tested on HrHRNet conditions				Tested on PETR conditions			
-	1 (best)	-	-	-	68.8	75.8	69.3	61.5	73.9	80.4	74.4	67.1
-	1 (test-gap)	-	-	-	69.8	76.6	70.3	62.8	74.7	80.9	75.1	67.9
-	1	1	1	1	68.9	76.0	69.4	61.5	74.4	80.7	74.8	67.6
-	15	-	-	-	71.4	78.0	71.8	64.5	75.9	81.9	76.3	69.1
1	15	1	1	1	70.9	77.7	71.5	63.9	75.5	81.7	75.9	68.9
+gen.	-	-	-	-	72.3	78.8	72.8	65.1	76.9	83.0	77.4	70.4

Table 4. Additional ablation studies for the number and type of different checkpoints during training. For empirical sampling, higher diversity (predictions sampled from different checkpoints of the bottom-up model) leads to better performance. We also found that generative sampling works well. "best" denotes the best performing checkpoint, while "test-gap" denotes the one for which training performance is closest to the final testing performance. All models are based on an HRNet-W32, are trained on input resolutions of 256x192 and tested with flipping.

Method	AP val	AP test
HGG (40)	35.6	34.8
HigherHRNet-W32 (15)	40.0	39.4
LOGO-CAP-W48 (41)	41.2	40.4
DEKR (16)	37.9	36.5
CID-W32 (32)	45.7	44.6
CID-W48 (32)	46.1	45.0
AlphaPose+ (31)	-	27.5
HRNet-W48* (7)	37.8	37.2
MIPNet-W48* (24)	42.0	42.5
BUCTD (HrHRNet-W32)†	44.1	43.5
BUCTD (CID-W32)†	47.3	46.3
BUCTD (CID-W32)† 2x	47.6	47.0
BUCTD (CID-W32)† 3x	47.7	47.2

Table 5. BUCTD improved performance on OCHuman. Comparison with state-of-the-art methods on the OCHuman val and test set after training on COCO train with conditions from an HigherHRNet-W32. † and * denotes input resolution of 256x192 and 384x288 respectively. Model in brackets denotes where conditions are coming from during inference. 2x and 3x marks iterative refinement by feeding back models predictions as new conditions. BUCTD models are with CoAM-W32; even with lower input resolution and the small HRNet-W32 we can outperform previous SOTA methods.

Method	AP	AP _M	AP _L
DEKR (16)	71.0	66.7	78.5
CID-W32 (32)	69.8	64.0	78.9
PETR (18)	73.1	67.2	81.7
HRNet-W48 (7)	76.3	72.3	83.4
MIPNet-W48 (24)	76.3	72.3	83.4
BUCTD (DEKR)	74.8	71.1	81.1
BUCTD (CID-W32)	74.8	71.1	81.1
BUCTD (PETR)	77.1	73.3	83.4
BUCTD (PETR)†	77.8	74.2	83.7
BUCTD (PETR)*	76.0	72.2	82.3
BUCTD (HRNet-W48)	76.5	72.7	83.2

Table 6. Results on the COCO val set. We beat or match every network when paired with BUCTD. †: BUCTD model with preNet, *: with TransPose, other BUCTD models are with CoAM-W48; all trained with generative sampling.

ods, but note that it has few overlapping people (24) compared to CrowdPose (8) and OCHuman (20).

Results. BUCTD outperforms well-performing single-stage, BU and TD methods (Table 6), using either BU or TD inputs as conditions (i.e., see within BU vs. TD improvements). This suggests that our method, designed for the challenges of

crowdedness, generalizes well to common pose estimation datasets, even with few overlapping persons. These results are also consistent with the insights from PoseFix (35) and PoseRefiner (36).

Multi-Animal Benchmarks

Datasets. To further assess the performance of BUCTD, we evaluated it on multi-animal benchmarks by Lauer et al. called SchoolingFish, Marmosets, and Tri-Mouse (17). These datasets impose different difficulties in the number of animals and crowdedness (Figure 4).

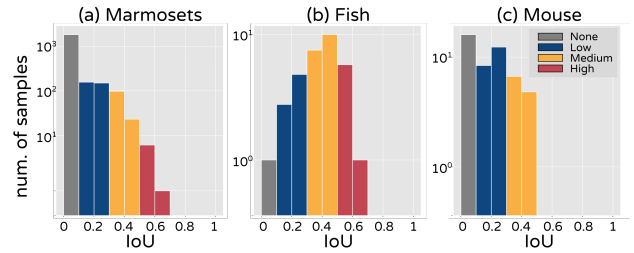


Fig. 4. Crowdedness levels in animal datasets, as divided into low, medium, and hard. The SchoolingFish (Fish) is the overall more crowded, while the Tri-Mouse (Mouse) is the least crowded dataset (IoU: Intersection Over Union).

Results. We trained BUCTD using the predictions from a bottom-up method based on DeepLabCut’s DLCRNet (17). We trained the TD models in the same way, so that bounding boxes of training and testing samples are computed from the predictions from DLCRNet. To compare the classic TD methods with an object detector, we also ran the TD models in a traditional way: training with ground truth bounding boxes, and testing the model with the bounding boxes from the object detectors (i.e., Faster R-CNN (2) and YOLOv3 (1)). Finally, we evaluated BUCTD-W32 and BUCTD-W48 methods and compared to the TD and BU methods. BUCTD outperforms the baseline methods on mice and marmosets and is competitive for fish. Furthermore, BUCTD strongly outperforms all other methods for crowded frames (Table 7, Figure 5).

Additionally, we trained the CTD model using the generative sampling scheme. During testing, we use the same pose inputs as for BUCTD models. These models also improves the performance on the three animal benchmarks (Table 7). However, compared to sampling the conditions from

	Marmosets				SchoolingFish				Tri-Mouse			
Method (detector)	AP	AP _L	AP _M	AP _H	AP	AP _L	AP _M	AP _H	AP	AP _L	AP _M	AP _H
Bottom-up methods												
Resnet (17)-AE (14)	45.0	-	-	-	40.0	-	-	-	70.3	-	-	-
HRNet (17)-AE (14)	65.1	-	-	-	45.7	-	-	-	83.9	-	-	-
DLCRNet (17)	80.1	75.3	71.9	67.5	74.1	68.7	77.6	72.8	95.8	94.9	94.7	-
CID-W32 (32)	92.5	90.5	91.8	82.9	81.0	72.7	84.0	79.9	86.8	84.1	85.6	-
Top-down methods												
HRNet-W48 (7) (YOLOv3 (1))	91.0	90.1	87.7	44.1	82.9	80.6	85.2	79.2	91.7	91.2	89.5	-
HRNet-W48 (7) (Faster R-CNN (2))	91.6	90.2	85.0	42.2	89.1	82.8	92.6	86.1	96.0	97.0	90.3	-
Hybrid approaches												
BUCTD-preNet-W48 (DLCRNet)	90.4	87.0	86.1	85.7	88.7	85.8	90.5	88.9	98.5	97.9	98.3	-
BUCTD-preNet-W48 (CID-W32)	93.3	91.9	93.4	89.9	88.0	79.3	90.4	90.5	87.7	85.6	87.3	-
BUCTD-CoAM-W48 (DLCRNet)*	91.6	86.3	88.9	89.4	81.9	71.0	81.0	78.3	99.1	99.1	99.2	-

Table 7. BUCTD performance on Animal Pose Datasets. Comparison with bottom-up and top-down model on animal benchmarks. BUCTD model largely outperforms the top-down methods in crowded scenes. Model in brackets denotes where conditions are coming from during inference. * denotes the generative sampling training scheme.

	Marmosets		SchoolingFish		Tri-Mouse	
Method	AP	AP _H	AP	AP _H	AP	AP _M
HRNet-W48 (YOLOv3)	91.0	44.1	82.9	79.2	91.7	89.5
BUCTD-CoAM-W32	91.3	45.5	87.8	85.0	94.9	91.5
BUCTD-CoAM-W48	91.3	48.0	86.3	82.1	92.4	90.5
BUCTD-preNet-W48	91.8	50.4	85.2	79.5	91.8	89.4
BUCTD-CoAM-W48 *	93.1	52.4	79.5	74.0	96.9	93.8
HRNet-W48 (FasterRCNN)	91.6	42.2	89.1	86.1	96.0	90.3
BUCTD-CoAM-W32	91.8	42.7	90.8	88.0	96.4	90.6
BUCTD-CoAM-W48	91.6	44.8	90.9	88.7	96.1	89.9
BUCTD-preNet-W48	91.8	44.8	89.3	87.4	96.3	91.9
BUCTD-CoAM-W48 *	92.8	49.8	85.0	81.0	97.3	92.5
DLCRNet	80.1	67.5	74.1	72.8	95.8	94.7
BUCTD-CoAM-W32	89.5	84.3	86.9	86.5	98.4	97.6
BUCTD-CoAM-W48	89.5	84.5	88.2	86.6	98.5	98.3
BUCTD-preNet-W48	90.4	85.7	88.7	88.9	98.5	98.3
BUCTD-CoAM-W48 *	91.6	89.4	81.9	78.3	99.1	99.2
CID-W32	92.5	82.9	81.0	79.9	86.8	85.6
BUCTD-CoAM-W32	93.1	84.0	86.3	85.4	90.9	88.0
BUCTD-CoAM-W48	92.9	86.3	87.2	83.8	90.2	88.1
BUCTD-preNet-W48	93.3	89.9	88.0	90.5	87.7	87.3
BUCTD-CoAM-W48 *	91.8	90.9	83.2	81.1	94.1	92.0

Table 8. Generalization results on animal benchmarks. All CTD models boosted the baseline results where the baseline results are used as conditional inputs for CTD model (trained on DLCRNet).

	Training box		Marmosets	SchoolingFish	Tri-Mouse
Method	GT	BU	AP	AP	AP
HRNet-W48	✓	-	85.2	73.0	97.5
HRNet-W48	-	✓	87.8	76.0	98.0
BUCTD-CoAM-W48	✓	-	85.8	78.9	98.3
BUCTD-CoAM-W48	-	✓	90.4	88.7	98.5

Table 9. Ablations to demonstrate the affect of training bounding boxes. Using bottom-up-computed (BU) boxes is more robust.

BU predictions (empirical sampling), this sampling strategy only performs well for marmosets and mice. The results on animals can vary with different CTD architectures.

We also compared the results based on the level of crowdedness.

Comparisons in different crowdedness levels. We calculated the Intersection Over Union (IoU) of the overlapped bounding boxes in the images and use the maximum IoU for each image (i.e., maxIoU) to indicate the crowdedness level. We then further split the test set into different crowdedness levels for the test set: low (S_L), medium (S_M) and high (S_H); Fig-

ure 4) to compute the metrics AP_L , AP_M , AP_H , respectively, to interrogate the model performance for different crowdedness levels test set (Table 7), where

$$S_L = \{I_i | i \in [1, n], \max Iou(I_i) \in [0.1, 0.3]\},$$

$$S_M = \{I_i | i \in [1, n], \max Iou(I_n) \in [0.3, 0.5]\},$$

$$S_H = \{I_i | i \in [1, n], \max Iou(I_n) > 0.5\}.$$

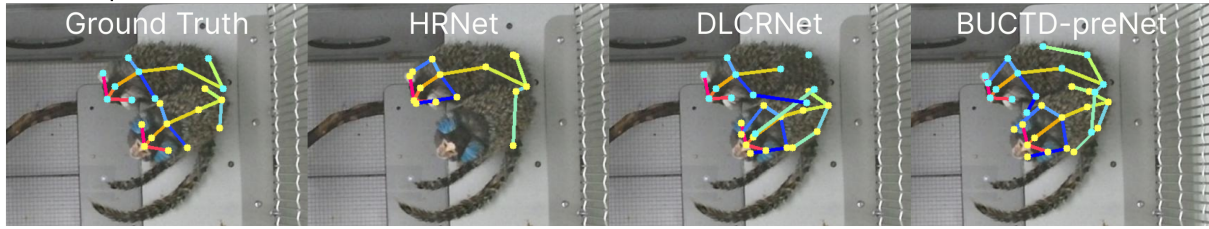
For the challenging AP_H division, BUCTD-W48 with preNet improved the performance on the Marmosets benchmark by up to 21.9 AP compared to other top-down approaches (BUCTD 89.4 AP vs. DLCRNet 67.5 AP and HRNet-W48 42.2 AP). BUCTD also improved the performance on the SchoolingFish AP_{hard} by up to 18.8 AP. In the Tri-Mouse dataset, BUCTD outperformed all tested methods (Table 7).

Ablation Results. One key questions is whether BUCTD is better because it is based on BU as a detector vs. a standard detectors or due to its pose-refinement ability. We show that for crowded scenes, BU detectors are key. To do so, we fed the pose predictions from top-down methods with standard detectors (YOLOv3, Faster R-CNN), to different CTD models; we found that they can further improve the performance (Table 8). This validates that CTD models can refine poses. Crucially, when considering the most challenging test data (AP_H/AP_M) then the results are substantially worse than for the full BUCTD pipeline. For instance, on difficult marmoset frames this method only reaches 52.4 mAP vs. 89.4 with BUCTD-CoAM-W48 (DLCRNet).

Next, to validate our design choices on the bounding boxes during training, we performed ablation studies for the BUCTD-CoAM-W48 model using the animal benchmarks.

The performance of top-down methods is influenced by the quality of the object detection outputs, i.e., the bounding boxes. Different from typical top-down methods which train the model based on ground truth bounding boxes, and test on detected bounding boxes. We trained the BUCTD model using bounding boxes computed from bottom-up predictions. Models trained on bottom-up-computed boxes perform the best on bottom-up-computed boxes during testing (Table 9).

(a) Comparison on Marmosets



(b) Results with BUCTD on SchoolingFish

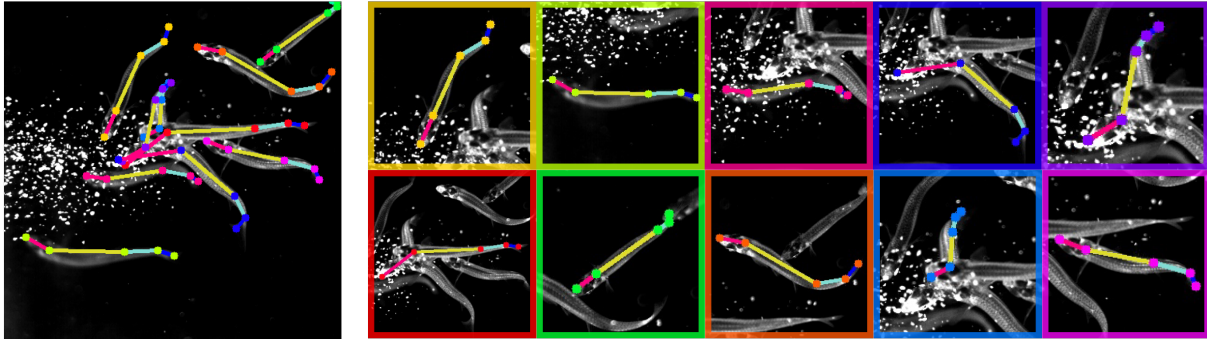


Fig. 5. Qualitative results on animal datasets. (a) Each image (left to right) shows the GT pose, HRNet-W48 predictions, DLCRNet predictions and BUCTD-preNet-W48 predictions. Due to crowdedness and occlusions, HRNet-W48 often missed the individual. DLCRNet may assign the body part to the wrong individual. BUCTD approach shows better performance in highly crowded conditions. (b) Results with BUCTD-preNet-W48.

Discussion

Humans and other animals often interact closely, and new solutions for accurately estimating poses in crowded scenes are needed. The field is increasingly moving towards benchmarks that encompass these challenges (8, 17, 20). Here, we present a new hybrid approach to improve multi-instance pose estimation especially in crowded scenarios. We compared our BUCTD method against classic bottom-up, top-down, and the newly proposed hybrid top-down method (MIPNet) which made great progress on crowded frames. Our BUCTD method achieves state-of-the-art performance on both CrowdPose and OCHuman. We believe the usage

of conditional input provided by a bottom-up pose estimator effectively helps in crowded scenes. Moreover, we tested our approach on three animal pose estimation benchmarks for their unique challenges of even more crowded data and show performance gains. For instance, on the challenging Schooling fish dataset we increased AP from 72.8 to 88.9.

Acknowledgements

We are grateful to EPFL and EPFL’s School of Life Sciences PTECH fund for proving funding. We thank Steffen Schneider, Shaokai Ye, Haozhe Qi, and other members of the Mathis Lab and Group for feedback.

References

1. Joseph Redmon and Ali Farhadi. Yolov3: An incremental improvement. *arXiv preprint arXiv:1804.02767*, 2018.
2. Shaoqing Ren, Kaiming He, Ross Girshick, and Jian Sun. Faster r-cnn: Towards real-time object detection with region proposal networks. *Advances in neural information processing systems*, 28, 2015.
3. Glenn Jocher et al. ultralytics/yolov5: v6.0 - YOLOv5n 'Nano' models, Roboflow integration, TensorFlow export, OpenCV DNN support. *Zenodo*, October 2021. doi: 10.5281/zenodo.5563715.
4. Ze Liu, Yutong Lin, Yue Cao, Han Hu, Yixuan Wei, Zheng Zhang, Stephen Lin, and Baining Guo. Swin transformer: Hierarchical vision transformer using shifted windows. *arXiv preprint arXiv:2103.14030*, 2021.
5. Hao-Shu Fang, Shuqin Xie, Yu-Wing Tai, and Cewu Lu. Rmpe: Regional multi-person pose estimation, 2018.
6. Zexin Chen, Ruihan Zhang, Yu Eva Zhang, Haowen Zhou, Hao-Shu Fang, Rachel R Rock, Aneesh Bal, Nancy Padilla-Coreano, Laurel Keyes, Kay M Tye, et al. AlphasTracker: a multi-animal tracking and behavioral analysis tool. *bioRxiv*, 2020.
7. Jingdong Wang, Ke Sun, Tianheng Cheng, Borui Jiang, Chaorui Deng, Yang Zhao, Dong Liu, Yadong Mu, Mingkui Tan, Xinggang Wang, Wenyu Liu, and Bin Xiao. Deep high-resolution representation learning for visual recognition, 2020.
8. Jiefeng Li, Can Wang, Hao Zhu, Yihuan Mao, Hao-Shu Fang, and Cewu Lu. Crowdpose: Efficient crowded scenes pose estimation and a new benchmark. In *Proceedings of the IEEE/CVF conference on computer vision and pattern recognition*, pages 10863–10872, 2019.
9. Sen Yang, Zhibin Quan, Mu Nie, and Wankou Yang. Transpose: Keypoint localization via transformer. In *Proceedings of the IEEE/CVF International Conference on Computer Vision*, pages 11802–11812, 2021.
10. Yanjie Li, Shoukui Zhang, Zhicheng Wang, Sen Yang, Wankou Yang, Shu-Tao Xia, and Erjin Zhou. Tokenpose: Learning keypoint tokens for human pose estimation. In *Proceedings of the IEEE/CVF International Conference on Computer Vision*, pages 11313–11322, 2021.
11. Yufei Xu, Jing Zhang, Qiming Zhang, and Dacheng Tao. ViTPose: Simple vision transformer baselines for human pose estimation. In Alice H. Oh, Alekh Agarwal, Danielle Belgrave, and Kyunghyun Cho, editors, *Advances in Neural Information Processing Systems*, 2022.
12. Eldar Insafutdinov, Mykhaylo Andriluka, Leonid Pishchulin, Siyu Tang, Evgeny Levinkov, Bjoern Andres, and Bernt Schiele. Articulated multi-person tracking in the wild. *CoRR*, abs/1612.01465, 2016.
13. Zhe Cao, Gines Hidalgo, Tomas Simon, Shih-En Wei, and Yaser Sheikh. Openpose: Real-time multi-person 2d pose estimation using part affinity fields, 2019.
14. Alejandro Newell, Zhiao Huang, and Jia Deng. Associative embedding: End-to-end learning for joint detection and grouping. *Advances in neural information processing systems*, 30, 2017.
15. Bowen Cheng, Bin Xiao, Jingdong Wang, Honghui Shi, Thomas S Huang, and Lei Zhang. Higherhrnet: Scale-aware representation learning for bottom-up human pose estimation. *Proceedings of the IEEE/CVF conference on computer vision and pattern recognition*, pages 5386–5395, 2020.
16. Zigang Geng, Ke Sun, Bin Xiao, Zhaoxiang Zhang, and Jingdong Wang. Bottom-up human pose estimation via disentangled keypoint regression. In *Proceedings of the IEEE/CVF Conference on Computer Vision and Pattern Recognition*, 2021.
17. Jessy Lauer, Mu Zhou, Shaokai Ye, William Menegas, Steffen Schneider, Tanmay Nath, Mohammed Mostafizur Rahman, Valentina Di Santo, Daniel Soberanes, Guoping Feng, et al. Multi-animal pose estimation, identification and tracking with deeplabcut. *Nature Methods*, 19(4):496–504, 2022.
18. Dahu Shi, Xing Wei, Liangqi Li, Ye Ren, and Wenming Tan. End-to-end multi-person pose estimation with transformers. In *Proceedings of the IEEE/CVF Conference on Computer Vision and Pattern Recognition*, pages 11069–11078, 2022.
19. Tsung-Yi Lin, Michael Maire, Serge Belongie, James Hays, Pietro Perona, Deva Ramanan, Piotr Dollár, and C Lawrence Zitnick. Microsoft coco: Common objects in context. In *European conference on computer vision*, pages 740–755. Springer, 2014.
20. Song-Hai Zhang, Ruilong Li, Xin Dong, Paul Rosin, Zixi Cai, Xi Han, Dingcheng Yang, Haozhi Huang, and Shi-Min Hu. Pose2seg: Detection free human instance segmentation. In *Proceedings of the IEEE/CVF Conference on Computer Vision and Pattern Recognition*, pages 889–898, 2019.
21. Kaiming He, Georgia Gkioxari, Piotr Dollár, and Ross Girshick. Mask r-cnn. In *Proceedings of the IEEE international conference on computer vision*, pages 2961–2969, 2017.
22. Weian Mao, Yongtao Ge, Chunhua Shen, Zhi Tian, Xinlong Wang, and Zhibin Wang. Tf-pose: Direct human pose estimation with transformers. *arXiv preprint arXiv:2103.15320*, 2021.
23. Mykhaylo Andriluka, Leonid Pishchulin, Peter Gehler, and Bernt Schiele. 2d human pose estimation: New benchmark and state of the art analysis. In *IEEE Conference on Computer Vision and Pattern Recognition (CVPR)*, June 2014.
24. Rawal Khirodkar, Visesh Chari, Amit Agrawal, and Ambrish Tyagi. Multi-instance pose networks: Rethinking top-down pose estimation. In *Proceedings of the IEEE/CVF International Conference on Computer Vision*, pages 3122–3131, 2021.
25. Mackenzie Weyand Mathis and Alexander Mathis. Deep learning tools for the measurement of animal behavior in neuroscience. *Current opinion in neurobiology*, 60:1–11, 2020.
26. Peiyun Hu and Deva Ramanan. Bottom-up and top-down reasoning with hierarchical rectified gaussians. In *CVPR*, pages 5600–5609, 2016.
27. Wei Tang, Pei Yu, and Ying Wu. Deeply learned compositional models for human pose estimation. In *ECCV*, pages 190–206, 2018.
28. Yujun Cai, Lihao Ge, Jun Liu, Jianfei Cai, Tat-Jen Cham, Junsong Yuan, and Nadia Magnenat Thalmann. Exploiting spatial-temporal relationships for 3d pose estimation via graph convolutional networks. In *ICCV*, pages 2272–2281, 2019.
29. Miaopeng Li, Zimeng Zhou, and Xinguo Liu. Multi-person pose estimation using bounding box constraint and lstm. *IEEE Transactions on Multimedia*, 21(10):2653–2663, 2019.
30. Yu Cheng, Bo Wang, and Robby T Tan. Dual networks based 3d multi-person pose estimation from monocular video. *IEEE Transactions on Pattern Analysis and Machine Intelligence*, 45(2):1636–1651, 2022.
31. Lingteng Qiu, Xuanye Zhang, Yanran Li, Guanbin Li, Xiaojun Wu, Zixiang Xiong, Xiaoguang Han, and Shuguang Cui. Peeking into occluded joints: A novel framework for crowd pose estimation. In *European Conference on Computer Vision*, pages 488–504. Springer, 2020.
32. Dongkai Wang and Shiliang Zhang. Contextual instance decoupling for robust multi-person pose estimation. In *Proceedings of the IEEE/CVF Conference on Computer Vision and Pattern Recognition*, pages 11060–11068, 2022.
33. Guillem Brasó, Nikita Kister, and Laura Leal-Taixé. The center of attention: Center-keypoint grouping via attention for multi-person pose estimation. In *Proceedings of the IEEE/CVF International Conference on Computer Vision*, pages 11853–11863, 2021.
34. Yiwei Ding, Wenjin Deng, Yinglin Zheng, Pengfei Liu, Meihong Wang, Xuan Cheng, Jianmin Bao, Dong Chen, and Ming Zeng. l^2 -r-net: Intra- and inter-human relation network for multi-person pose estimation. In Luc De Raedt, editor, *Proceedings of the Thirty-First International Joint Conference on Artificial Intelligence, IJCAI 2022, Vienna, Austria, 23-29 July 2022*, pages 855–862. ijcai.org, 2022. doi: 10.24963/ijcai.2022/120.
35. Gyeonsik Moon, Ju Yong Chang, and Kyoung Mu Lee. Posefix: Model-agnostic general human pose refinement network. In *Proceedings of the IEEE/CVF Conference on Computer Vision and Pattern Recognition*, pages 7773–7781, 2019.
36. Mihai Fieraru, Anna Khoreva, Leonid Pishchulin, and Bernt Schiele. Learning to refine human pose estimation. In *Proceedings of the IEEE conference on computer vision and pattern recognition workshops*, pages 205–214, 2018.
37. Matteo Ruggero Ronchi and Pietro Perona. Benchmarking and error diagnosis in multi-instance pose estimation. In *Proceedings of the IEEE international conference on computer vision*, pages 369–378, 2017.
38. Jun Fu, Jing Liu, Haijie Tian, Yong Li, Yongjun Bao, Zhiwei Fang, and Hanqing Lu. Dual attention network for scene segmentation. In *Proceedings of the IEEE/CVF conference on computer vision and pattern recognition*, pages 3146–3154, 2019.
39. Bruno Artacho and Andreas Savakis. Bapose: Bottom-up pose estimation with disentangled waterfall representations. *arXiv preprint arXiv:2112.10716*, 2021.
40. Sheng Jin, Wentao Liu, Enze Xie, Wenhai Wang, Chen Qian, Wanli Ouyang, and Ping Luo. Differentiable hierarchical graph grouping for multi-person pose estimation. In *European Conference on Computer Vision*, pages 718–734. Springer, 2020.
41. Nan Xue, Tianfu Wu, Gui-Song Xia, and Liangpei Zhang. Learning local-global contextual adaptation for multi-person pose estimation. In *Proceedings of the IEEE/CVF Conference on Computer Vision and Pattern Recognition*, pages 13065–13074, 2022.
42. MMPose Contributors. Openmmlab pose estimation toolbox and benchmark. <https://github.com/open-mmlab/mmpose>, 2020.
43. Diederik P Kingma and Jimmy Ba. Adam: A method for stochastic optimization. *arXiv preprint arXiv:1412.6980*, 2014.
44. Kai Chen, Jiaqi Wang, Jiangmiao Pang, Yuhang Cao, Yu Xiong, Xiaoxiao Li, Shuyang Sun, Wansen Feng, Ziwei Liu, Jiarui Xu, Zheng Zhang, Dazhi Cheng, Chenchen Zhu, Tianheng Cheng, Qijie Zhao, Buyu Li, Xin Lu, Rui Zhu, Yue Wu, Jifeng Dai, Jingdong Wang, Jianping Shi, Wanli Ouyang, Chen Change Loy, and Dahua Lin. MMDetection: Open mmlab detection toolbox and benchmark. *arXiv preprint arXiv:1906.07155*, 2019.

Supplementary Materials

Contents

A Implementation details.	11
A.1 Training settings for bottom-up pose detectors.	11
A.2 Training settings for conditional top-down (CTD) pose estimators.	11
A.3 Design of the conditional input to CTD.	11
A.4 Details of generative sampling scheme during conditional training.	11
B Contrasting BU-based detectors and vanilla detectors.	13
B.1 Evaluation on ground-truth bounding boxes.	13
B.2 Performance details - precision and recall.	13
B.3 Robustness to number of detections.	13
C Computational costs of training BUCTD.	13
D Success and failure cases.	14

In the following, we provide implementation details, compare the general detection performance of the bottom-up stage, and evaluate the type of conditional training data that gives best CTD results. We conclude by showing that the computational costs of BUCTD compare favorably to the standard detector and TD pipeline, as well as success and failure cases of the BUCTD model.

Overall, our work demonstrated that providing individual detections and conditional pose input derived from a bottom-up pose detector to a Conditional Pose Estimator (CTD) can effectively boost performance in crowded scenes.

Supplementary Note A: Implementation details.

We report training and implementation details for the bottom-up and the conditional top-down models applied to both human benchmarks and animal benchmarks.

A.1. Training settings for bottom-up pose detectors.

In order to create pose proposals from bottom-up models, we trained DLCRNet-ms4 (17) on the animal benchmarks, and HigherHRNet-W32 using mmpose (42) on the human benchmarks. We show the default training settings in Table S1.

Note that the HigherHRNet-W32 is trained with the exact same setting for both COCO (19) (for inference on OCHuman (20)) and CrowdPose (8). We furthermore used the same settings as the DLCRNet on all three animal datasets (Table S1).

A.2. Training settings for conditional top-down (CTD) pose estimators. Here we provide the default parameter settings for CTD-CoAM-W32/48 and CTD-TP-H-A6 trained on human benchmarks (Table S2).

During training on the animal benchmarks, we used the same settings for CTD-CoAM-W32/W48 (Table S2). However, to keep the aspect ratio for animals, we pad the cropped

individuals to the input resolution of 256×256 and set the batch size to 16.

For training CTD-CoAM-W32 on COCO (19), we train for 110 epochs, with an initial learning rate of 0.02 and a learning rate drop at epochs 70 and 110, respectively.

A.3. Design of the conditional input to CTD. The condition fed to the CTD stage of our BUCTD framework is created as follows. With the predictions coming from the first stage, we generate a conditional heatmap in ($c \in \mathbf{R}^{H \times W \times 3}$) by using a Gaussian distribution with a standard deviation σ . We tried several variants for this conditional input: color heatmap (CM), gray-scale heatmap (GM), and K-channel single Gaussian heatmaps (KM). We achieved +1.3 mAP with CM, +0.9 mAP with GM, vs KM CoAM-W32 on CrowdPose. Therefore, we applied color heatmap as conditions for the CoAM module.

A.4. Details of generative sampling scheme during conditional training. Similar to PoseFix (35), during training, we synthesized the pose by using the error statistics described in Ronchi and Perona (37) to generate noisy pose as conditional inputs. We generated the conditional pose with the four error types of jitter, inversion, swap and miss. For human benchmark, i.e. CrowdPose, we applied the same error probabilities as in PoseFix (which are estimated from COCO and are likely slightly different (37); despite this we achieve excellent results). For animal benchmarks, we utilized the same error types and tuned the error distribution by running a few different cases; we ended up using jitter error: 0.15 or

Hyperparameters	Animal Benchmarks	
	DLCRNet	HrHRNet-W32
Optimizer	Adam (43)	Adam (43)
Base learning rate	0.0001	0.0015
Learning rate sched.	step [7500, 12000]	step [200, 260]
Learning rate drop (γ)	[0.5, 0.2]	0.1
Training epochs	-	300
Training iterations	60,000	-
Warmup iterations	-	500
Warmup ratio	-	0.001
Batch size	8	40
Input resolution	400×400	512×512
Rotation	24°	30°
Scale	[0.5, 1.25]	[0.75, 1.5]
RandomFlip	-	0.5

Table S1. Default training settings for bottom-up models. We applied these hyperparameters and training data settings to the bottom-up models (DLCRNet for animal datasets, and HigherHRNet for human benchmarks).

Hyperparameters	CTD-CoAM-W32/48	
	CTD-CoAM-W32/48	CTD-TP-H-A6
Optimizer	Adam (43)	Adam (43)
Base learning rate	0.001	0.0001
Weight decay	0.0001	0.1
Learning rate sched.	step [170,200]	step [100,150,200,220]
Learning rate drop (γ)	0.1	0.25
Training epochs	210	240
Batch size	96/48	64
Input resolution	$256 \times 192 / 384 \times 288$	256×192
Rotation	45°	45°
Scale	[0.65, 1.35]	[0.65, 1.35]
RandomFlip	0.5	0.5

Table S2. Default training settings for conditional top down models. We apply these hyperparameters and training data settings to a CTD-CoAM-W32.



Fig. S1. Additional predictions using BUCTD-CoAM-W48 with conditional inputs from PETR on the CrowdPose *test* set.

0.2 (depending on keypoint validity), miss error: 0.05 or 0.2 (depending on keypoint validity), inversion error: 0.03, swap error: 0.04 or 0.1 (depending on keypoint validity). Additionally, we allow swapping keypoints between individuals that do not have any overlap, to simulate wrong assemblies in the bottom-up stage.

Our results demonstrate that the CoAM module leads to improved performance on some animal benchmarks when applying generative sampling (Table S3). However, the preNet module underperforms on the SchoolingFish dataset compared to the baseline results. We further ablate the er-

ror types and find that the performance with fewer error types on preNet-W48 on the SchoolingFish dataset is slightly higher than the performance on the models with all error types. Specifically, when we use two types of errors (jitter and swap), we achieve 71.7 AP, while using jitter error only results in 77.0 AP.

From the different results, we speculate that the generative sampling strategy is not as stable as empirical sampling on difficult, small-scale datasets (e.g., fish), likely due to different error statistics between human and animal pose estimation methods. However, combined generative and empirical sampling could be a great strategy to explore in the future.

methods	Marmosets	Sch.Fish	Tri-Mouse
BUCTD-preNet-W48 (DLCRNet)	91.6	62.1	98.4
BUCTD-CoAM-W48 (DLCRNet)	91.6	81.9	99.1
BUCTD-preNet-W48 (DLCRNet)*	90.4	88.7	98.5

Table S3. Results on animal benchmarks with generative sampling and empirical sampling. * denotes empirical sampling.

Supplementary Note B: Contrasting BU-based detectors and vanilla detectors.

In this section, we compare our method with previous SOTA (MIPNet) based on precision and recall. We find higher performance on both metrics with BUCTD, also strong error-correcting capabilities to improve the performance of BU models.

Furthermore, to ablate the influence of the number of detections (which vary widely across different BU models), we only provide the same (amount of) detected bounding boxes as in MIPNet to our CTD models. We notice that our method still outperforms MIPNet, independent of the bottom-up model applied, and with especially large gains on hard frames (i.e. frames with higher crowdedness level).

B.1. Evaluation on ground-truth bounding boxes. First, to take the detectors completely out of the equation, we simply evaluated different models on ground truth bounding boxes (i.e., the same pixel input).

Method	AP	AP _{easy}	AP _{med}	AP _{hard}
HRNet-W32 (7)	70.0	78.8	70.3	61.7
MIPNet-W32 (24)	71.2	78.8	71.5	63.8
BUCTD-CoAM-W32 (Ours)	75.2	81.4	75.3	70.7

Table S4. Our BUCTD model outperforms HRNet and MIPNet on CrowdPose *val* (using ground-truth bounding boxes). All models are trained on input resolutions of 256x192.

We compare the performance of our BUCTD-CoAM-W32 model on CrowdPose to HRNet and MIPNet when evaluated using ground-truth bounding boxes (Table S4). Note that these models were trained on *train* and validated on *val* (as done in (24)). During training we matched the conditions to the GT keypoints and then fed it to the CTD model together with the input crop. The same approach is used during testing. Our method outperforms the HRNet baseline and improves upon the MIPNet baseline, that was designed to better handle crowded scenarios. While MIPNet only achieves small improvements over HRNet, our method substantially boosts the AP values, especially on the hard, very crowded cases (+ 9.0 AP over HRNet and + 6.9 AP over MIPNet). This directly corroborates our choice to provide conditional pose input to boost performance.

B.2. Performance details - precision and recall. To gain better insights into the performance gains of BUCTD, we computed the precision and recall values on the CrowdPose (Fig. S2) test set. We compare our model (trained with empirical sampling) to the previous SOTA on CrowdPose: MIPNet. Importantly, we have higher recall and precision than MIPNet for all models. Thus, due to its careful design, BUCTD improves the precision and recall for all BU models we tested.

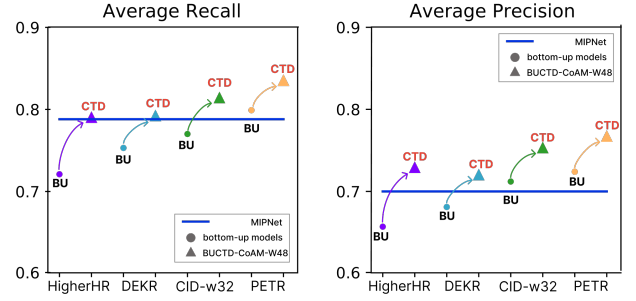


Fig. S2. Comparison of recall and precision curves for different BU and CTD models vs. MIPNet. CTD boosts both precision and recall (of BU models), and can thus “recover” more poorly predicted persons than MIPNet.

B.3. Robustness to number of detections. Next, we wanted to fairly compare our BUCTD in terms on number of detections the first stage provides, in order to exclude that simply a higher number of detections, made by the bottom-up pose detector in comparison to commonly used object detectors, would lead to our superior performance. We hence provided the *same number* of detections from both the bottom-up models and an object detector; despite this artificial constraint the performance of BUCTD was still significantly higher than the one of MIPNet (24) (Figure S3).

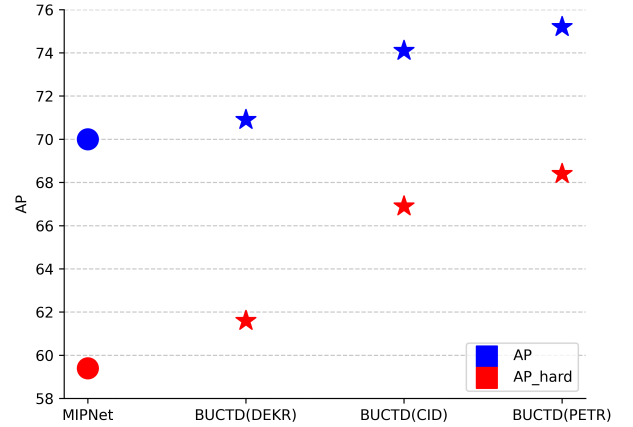


Fig. S3. Performance of BUCTD when provided with same amount of detections (65,044) as the object detector of MIPNet. When constraining the number of detections we pass from our bottom-up pose detector (DEKR, CID, PETR) to the CTD model to the same amount of detections MIPNet receives from the object detector on the CrowdPose test set, our BUCTD framework still significantly outperforms MIPNet on AP and AP_{hard}.

Supplementary Note C: Computational costs of training BUCTD.

There are three components for creating a BUCTD model (and comparing it to the standard pipeline either BU or detector + TD). Naturally, simply using a BU model is more efficient, but we also achieve more accuracy. In contrast, BU models are more efficient than detectors (as we show below). Creating and storing the empirical predictions as well as matching them to ground-truth also comes with some cost



Fig. S4. Example failure cases from the CrowdPose *test* set. Especially in very occluded scenarios and complex sport scenes, our BUCTD-CoAM-W48 model sometimes shows inaccuracies in estimating the correct position of the extremities. Errors are highlighted by yellow ellipses.

Method	#params	GFLOPs
Stage 1		
FasterRCNN	60.0M	246.0
YOLOv3	62.0M	65.9
HigherHR.W32	28.6M	47.9
DEKR	28.6M	44.5
CID	29.4M	43.2
PETR	220.5M	-
Stage 2		
HRNet-W48	63.6M	19.5
MIPNet-W48	63.7M	64.5
PoseFix	68.7M	36.6
BUCTD-preNet-W32	28.5M	7.6
BUCTD-TP-H-A6	17.0M	8.4
BUCTD-CoAM-W32	39.1M	8.6
BUCTD-CoAM-W48	115.6M	43.5

Table S5. Number of parameters and GFLOPs on stage 1 (object detectors, bottom-up models), and stage 2 (top-down models and our methods).

(while one does not have this costs with generative sampling, one might need to estimate the error distribution), but training CTD or TD models is comparable. Furthermore, inference of TD and CTD is also comparable (with an advantage for TD). However, those costs come at the benefit of stronger performance – in applications the latter can be much more important.

We compared the parameters and GFLOPs on object detectors, bottom-up models, top-down models and our methods in Table S5. Bottom-up models have generally less parameters and GFLOPs than object detectors. We further compare the overall training time of object detectors vs. bottom-up pose detectors. We trained two commonly used object detectors (i.e. Faster R-CNN (2) and YOLOv3 (1)) with the default parameter settings from mmdetection (44) and a DL-CRNet (17) as the bottom-up pose detector on the animal benchmarks. For training on the marmosets datasets, training the FasterRCNN detector with 90 epochs took 26.5 hours (saturated around 60 epochs), training the YOLOv3 with 273 epochs took 33 hours (saturated around 258 epochs). However, training the DL-CRNet took only 2.25 hours for 90 epochs. Experiments were performed on a single Titan RTX. Compared to training the object detectors, suggests that training the bottom-up models requires less training time.

Supplementary Note D: Success and failure cases.

To further illustrate the power of our method, we show additional qualitative results of success (Figure S1) and failure cases (Figure S4).